Deflection and trapping of spatial solitons in linear photonic potentials

Chandroth P. Jisha,[1*] Alessandro Alberucci,[2] Ray-Kuang Lee,[3] and Gaetano Assanto[2]

[1]*Centro de Física do Porto, Faculdade de Ciências, Universidade do Porto, R. Campo Alegre 687, Porto 4169-007, Portugal*

[2]*Nonlinear Optics and OptoElectronics Lab (NooEL), Via della Vasca Navale 84, 00146 Rome, Italy*

[3]*Institute of Photonics Technologies, National Tsing-Hua University, Hsinchu 300, Taiwan*

[*] *cpjisha@gmail.com*

Abstract: We investigate the dynamics of spatial optical solitons launched in a medium with a finite perturbation of the refractive index. For longitudinally short perturbations of super-Gaussian transverse profile, as the input power varies we observe a transition from a wave-like behavior where solitons break up into multiple fringes to a particle-like behavior where solitons acquire a transverse velocity retaining their shape. For longitudinally long perturbations with an attractive potential solitons get trapped inside the well and propagate with transverse periodic oscillations, resulting in an efficient power-dependent angular steering or deflection. Using the Ehrenfest theorem we derive analytical expressions for soliton trajectory, and achieve excellent agreement between theory and numerical simulations for large powers, that is, narrow solitons.

OCIS codes: (190.0190) Nonlinear optics; (190.6135) Spatial solitons; (260.5950) Self-focusing; (260.2710) Inhomogeneous optical media.

References and links

1. A. Amo, S. Pigeon, D. Sanvitto, V. G. Sala, R. Hivet, I. Carusotto, F. Pisanello, G. Lemnager, R. Houdr, E. Giacobino, C. Ciuti, and A. Bramati, "Polariton superfluids reveal quantum hydrodynamic solitons," Science **332**, 1167–1170 (2011).
2. C. P. Jisha, Y. Lin, T.-D. Lee, and R.-K. Lee, "Crescent waves in optical cavities," Phys. Rev. Lett. **107**, 183902 (2011).
3. I. Carusotto and C. Ciuti, "Quantum fluids of light," Rev. Mod. Phys. **85**, 299–366 (2013).
4. G. I. Stegeman and M. Segev, "Optical spatial solitons and their interactions: Universality and diversity," Science **286**, 1518–1523 (1999).
5. A. B. Aceves, J. V. Moloney, and A. C. Newell, "Theory of light-beam propagation at nonlinear interfaces. i. equivalent-particle theory for a single interface," Phys. Rev. A **39**, 1809–1827 (1989).
6. A. B. Aceves, J. V. Moloney, and A. C. Newell, "Theory of light-beam propagation at nonlinear interfaces. ii. multiple-particle and multiple-interface extensions," Phys. Rev. A **39**, 1828–1840 (1989).
7. L. Friedrich, G. I. Stegeman, P. Millar, C. J. Hamilton, and J. S. Aitchison, "Dynamic, electronically controlled angle steering of spatial solitons in AlGaAs slab waveguides," Opt. Lett. **23**, 1438–1440 (1998).
8. M. Peccianti, A. Dyadyusha, M. Kaczmarek, and G. Assanto, "Tunable refraction and reflection of self-confined light beams," Nat. Phys. **2**, 737–742 (2006).
9. B. Alfassi, C. Rotschild, O. Manela, M. Segev, and D. N. Christodoulides, "Nonlocal surface-wave solitons," Phys. Rev. Lett. **98**, 213901 (2007).
10. M. Peccianti, G. Assanto, A. Dyadyusha, and M. Kaczmarek, "Non-specular total internal reflection of spatial solitons at the interface between highly birefringent media," Phys. Rev. Lett. **98**, 113902 (2007).

#191688 - $15.00 USD Received 3 Jun 2013; revised 17 Jul 2013; accepted 20 Jul 2013; published 29 Jul 2013

11. A. Piccardi, G. Assanto, L. Lucchetti, and F. Simoni, "All-optical steering of soliton waveguides in dye-doped liquid crystals," Appl. Phys. Lett. **93**, 171104 (2008).
12. A. Barak, O. Peleg, C. Stucchio, A. Soffer, and M. Segev, "Observation of soliton tunneling phenomena and soliton ejection," Phys. Rev. Lett. **100**, 153901 (2008).
13. Y. Linzon, R. Morandotti, M. Volatier, V. Aimez, R. Ares, and S. Bar-Ad, "Nonlinear scattering and trapping by local photonic potentials," Phys. Rev. Lett. **99**, 133901 (2007).
14. A. Alberucci, M. Peccianti, and G. Assanto, "Nonlinear bouncing of nonlocal spatial solitons at the boundaries," Opt. Lett. **32**, 2795–2797 (2007).
15. M. Peccianti, A. Dyadyusha, M. Kaczmarek, and G. Assanto, "Escaping solitons from a trapping potential," Phys. Rev. Lett. **101**, 153902 (2008).
16. A. Alberucci, A. Piccardi, U. Bortolozzo, S. Residori, and G. Assanto, "Nematicon all-optical control in liquid crystal light valves," Opt. Lett. **35**, 390–392 (2010).
17. C. P. Jisha, A. Alberucci, R.-K. Lee, and G. Assanto, "Optical solitons and wave-particle duality," Opt. Lett. **36**, 1848–1850 (2011).
18. A. Alberucci, G. Assanto, A. A. Minzoni, and N. F. Smyth, "Scattering of reorientational optical solitary waves at dielectric perturbations," Phys. Rev. A **85**, 013804 (2012).
19. A. B. Aceves, C. De Angelis, T. Peschel, R. Muschall, F. Lederer, S. Trillo, and S. Wabnitz, "Discrete self-trapping, soliton interactions, and beam steering in nonlinear waveguide arrays," Phys. Rev. E **53**, 1172–1189 (1996).
20. F. Lederer, G. I. Stegeman, D. N. Christodoulides, G. Assanto, M. Segev, and Y. Silberberg, "Discrete solitons in optics," Phys. Rep. **463**, 1–126 (2008).
21. V. A. Brazhnyi, C. P. Jisha, and A. S. Rodrigues, "Interaction of discrete nonlinear Schrödinger solitons with a linear lattice impurity," Phys. Rev. A **87**, 013609 (2013).
22. R. Morandotti, H. S. Eisenberg, D. Mandelik, Y. Silberberg, D. Modotto, M. Sorel, C. R. Stanley, and J. S. Aitchison, "Interactions of discrete solitons with structural defects," Opt. Lett. **28**, 834–836 (2003).
23. A. Fratalocchi and G. Assanto, "Symmetry-breaking instabilities in perturbed optical lattices: Nonlinear nonreciprocity and macroscopic self-trapping," Phys. Rev. A **75**, 063828 (2007).
24. V. V. Konotop, D. Cai, M. Salerno, A. R. Bishop, and N. Grønbech-Jensen, "Interaction of a soliton with point impurities in an inhomogeneous, discrete nonlinear Schrödinger system," Phys. Rev. E **53**, 6476–6485 (1996).
25. L. Morales-Molina and R. A. Vicencio, "Trapping of discrete solitons by defects in nonlinear waveguide arrays," Opt. Lett. **31**, 966–968 (2006).
26. J. Cuevas, B. A. Malomed, and P. G. Kevrekidis, "Motion of discrete solitons assisted by nonlinearity management," Phys. Rev. E **71**, 066614 (2005).
27. G. Assanto, L. A. Cisneros, A. A. Minzoni, B. D. Skuse, N. F. Smyth, and A. L. Worthy, "Soliton steering by longitudinal modulation of the nonlinearity in waveguide arrays," Phys. Rev. Lett. **104**, 053903 (2010).
28. K. Forinash, M. Peyrard, and B. Malomed, "Interaction of discrete breathers with impurity modes," Phys. Rev. E **49**, 3400–3411 (1994).
29. I. L. Garanovich, S. Longhi, A. A. Sukhorukov, and Y. S. Kivshar, "Light propagation and localization in modulated photonic lattices and waveguides," Physics Reports **518**, 1–79 (2012).
30. A. Alberucci, C. P. Jisha, R.-K. Lee, and G. Assanto, "Soliton self-routing in a finite photonic potential," Opt. Lett. **38**, 2071–2073 (2013).
31. X. D. Cao and B. A. Malomed, "Soliton-defect collisions in the nonlinear Schrödinger equation," Phys. Lett. A **206**, 177–182 (1995).
32. P. Y. P. Chen, B. A. Malomed, and P. L. Chu, "Trapping bragg solitons by a pair of defects," Phys. Rev. E **71**, 066601 (2005).
33. S. Garzia, C. Sibilia, and M. Bertolotti, "Swing effect of spatial solitons," Opt. Comm. **139**, 193–198 (1997).
34. L. W. Dong and H. Wang, "Oscillatory behavior of spatial soliton in a gradient refractive index waveguide with nonlocal nonlinearity," Appl. Phys. B **84**, 465–469 (2006).
35. Y. S. Kivshar and G. P. Agrawal, *Optical Solitons* (Academic, 2003).
36. J. J. Sakurai, *Modern Quantum Mechanics* (Addison-Wesley, 1994).
37. Y. S. Kivshar and B. A. Malomed, "Dynamics of solitons in nearly integrable systems," Rev. Mod. Phys. **61**, 763–915 (1989).
38. V. Serkin, A. Hasegawa, and T. Belyaeva, "Geiger–nuttall law for Schrödinger solitons," J. Mod. Opt. **60**, 116–127 (2013).
39. G. Assanto, A. A. Minzoni, and N. F. Smyth, "Nematicons escaping a wide trapping potential: modulation theory," Phys. Rev. A **79**, 033837 (2009).
40. M. Peccianti and G. Assanto, "Nematicons," Phys. Rep. **516**, 147–208 (2012).

#191688 - $15.00 USD Received 3 Jun 2013; revised 17 Jul 2013; accepted 20 Jul 2013; published 29 Jul 2013

1. Introduction

Scattering and transmission of light beams by inhomogenities of the medium are fundamental phenomena and have been widely investigated in both linear and nonlinear regimes [1–3]. The dynamics of spatial optical solitons, i.e. transversely localized nonlinear wavepackets [4], at the interface between media has been addressed as well, both experimentally and theoretically [5–12]. Aceves et al. adopted a particle approach to model reflection and transmission of an obliquely incident beam propagating through a nonlinear interface [5], even in the cases of multiple beams or multiple interfaces [6]. It was demonstrated that spatial solitons are robust enough to survive transitions at the interface, including total internal reflection [8, 10, 11], trapping and scattering [13, 14], tunneling and escaping [12, 15]. Since the resulting soliton trajectory depends on power, some of these features have suggested their use for all-optical switching and computing [16–18].

Interactions of optical solitons with defects have also been studied in discrete waveguide arrays [19–21]. The effects of either attractive or repulsive defects were studied by considering increases or decreases in coupling strength [22, 23], linear or nonlinear impurities in the array [24, 25] as well as longitudinal modulations of the nonlinearity [26, 27]. The interaction of discrete breathers with impurtiy modes can lead to interesting phenomena such as fusion [28].

The aim of this work is to study the dynamics of optical spatial bright solitons (hereafter simply called solitons) propagating in a medium in the presence of a finite linear perturbation of the refractive index associated to a localized *photonic potential* [13, 29, 30]. Such index inhomogeneity can affect the soliton dynamics [31, 32], including oscillations with period depending on power in either saturating [33] or nonlocal media [34]. Moreover, we recently demonstrated that by varying the ratio between the widths of the input beam and the defect one can observe wave-particle dualism asssociated to the soliton-defect interaction [17, 18]. When the ratio is large, i.e. the soliton is much wider than the tranverse size of the photonic potential, the phase of the beam is modulated by the defect resulting in beam breakup into multiple fringes; when the soliton is much narrower than the defect (i.e. a narrow soliton), the beam maintains its shape and can be steered, i.e. its trajectory can be controlled by power, an interesting phenomenon towards all-optical processing architectures. Hereby we characterize the interaction of a soliton with a photonic potential of finite size in both transverse and longitudinal coordinates, specifically addressing soliton splitting and steering. Even though our results concern optics, they can be adapted and applied to other fields, particularly to Bose-Einstein condensates where the condensate density plays the role of the light wavepacket.

The paper is organized as follows: in section 2, starting from the Ehrenfest theorem, we develop a general model (i.e., independent on the specific nonlinearity) for the soliton trajectory in inhomogeneous nonlinear media; in section 3 we present numerical simulations of soliton dynamics in both repulsive as well as attractive defects, for various profiles of the linear photonic potential; in section 4 we extend the analysis to the study of breathers and their propagation in a potential. In all cases we compare numerics and analytical predictions to show their good agreement, particulary for narrow solitons.

2. Ehrenfest theorem for solitons

Starting from Maxwell's equations in the harmonic regime in isotropic media, neglecting the divergence of the electric field it is possible to derive that the electric field satisfies a vectorial Helmholtz equation:

$$(\nabla^2 + k_0^2 n^2)\mathbf{E}(x,y,z) = 0, \tag{1}$$

where $n = n_0 + n_L(x,y) + n_2|\mathbf{E}|^2$ is the overall distribution of the refractive index, with n_0 the

#191688 - $15.00 USD Received 3 Jun 2013; revised 17 Jul 2013; accepted 20 Jul 2013; published 29 Jul 2013

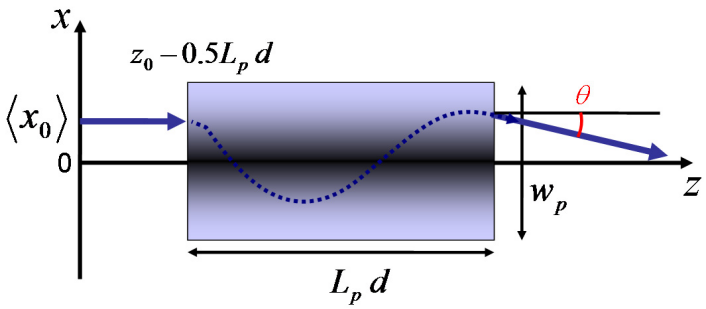

Fig. 1. Sketch of the soliton interaction (blue arrow) with a finite linear photonic potential (box) of width w_p across x and of length $L_p d$ along z (units in the laboratory frame). A soliton is launched along the axis z in ($x = \langle x_0 \rangle$, $z = 0$). After the interaction the soliton emerges with a finite angle θ depending on both beam power and input location. In the sketched example the defect has a positive index increase (darker area) and is able to transversely trap the beam.

linear index, n_L the linear (i.e., independent from light) perturbation in index, n_2 the nonlinear Kerr coefficient. Thus in Eq. (1) we can write $n^2 = n_0^2 + 2n_0 n_L + 2n_0 n_2 |E|^2$ in the limit of small perturbations. Assuming linearly polarized beams we can write $E = A(x,y,z)\exp(ik_0 n_0 z)$, where $k_0 = 2\pi/\lambda$ is the vacuum wavenumber. For the sake of simplicity we also limit the analysis to only one transverse dimension by setting $\partial_y = 0$. For paraxial wave propagation along the axis z, Eq. (1) reduces to the scalar wave equation in $(1+1)$D

$$2ik_0 n_0 \frac{\partial A}{\partial z} + \frac{\partial^2 A}{\partial x^2} + 2k_0^2 n_0 n_L A + 2k_0^2 n_0 n_2 |A|^2 A = 0, \tag{2}$$

where we took $|n_L| \ll n_0$. Defining $Z = z/L_p$, $X = x/w_p$, $u = \sqrt{2pn_0 n_2}A$, $L_p = k_0 w_p^2 n_0$ and labelling w_p the width of the defect, Eq. (2) can be recast as

$$i\frac{\partial u}{\partial Z} + \frac{1}{2}\frac{\partial^2 u}{\partial X^2} + |u|^2 u - pV_{\text{eff}}(X,Z)\,u = 0, \tag{3}$$

with $p = k_0^2 w_p^2/2$ and $V_{\text{eff}} = -2n_0 n_L(X,Z) = -\Delta \exp\left(-X^{2l}\right) \text{rect}_d(Z - Z_0)$, where $\Delta/\left(k_0^2 w_p^2 n_0\right)$ is the increase/decrease in linear index (i.e. positive/negative resulting in an attractive/repulsive defect, respectively), d is the defect extension along Z and l is a positive integer related to the abruptness of head and tail in $n_L(X,Z)$. Hereby we consider photonic potentials with longitudinally invariant shape (along Z) and even symmetry across X (see sketch in Fig. 1). The input wavepacket is a Kerr soliton $u(X, Z=0) = Nu_0 \text{sech}(u_0 X)$, the integer N spanning the soliton order ($N = 1$ fundamental soliton, $N > 1$ higher order solitons [35]).

The dynamics of the soliton beam, after interacting with the linear defect, can be appreciated using the Ehrenfest theorem [36], which provides the expectation value for the beam position as

$$\frac{d^2\langle X \rangle}{dZ^2} = -p \int \psi \frac{\partial V_{\text{eff}}}{\partial X} dX, \tag{4}$$

with $\psi = |u|^2 / \int |u|^2 dX$ the normalized intensity and $\langle X \rangle = \int \psi X dX$ the beam position. Owing to symmetry, the contribution of the nonlinear potential is zero as long as it is symmetric with respect to the beam axis $\langle X \rangle$: in this limit the right hand side of Eq. (4) depends only on the linear index distribution n_L.

#191688 - $15.00 USD Received 3 Jun 2013; revised 17 Jul 2013; accepted 20 Jul 2013; published 29 Jul 2013

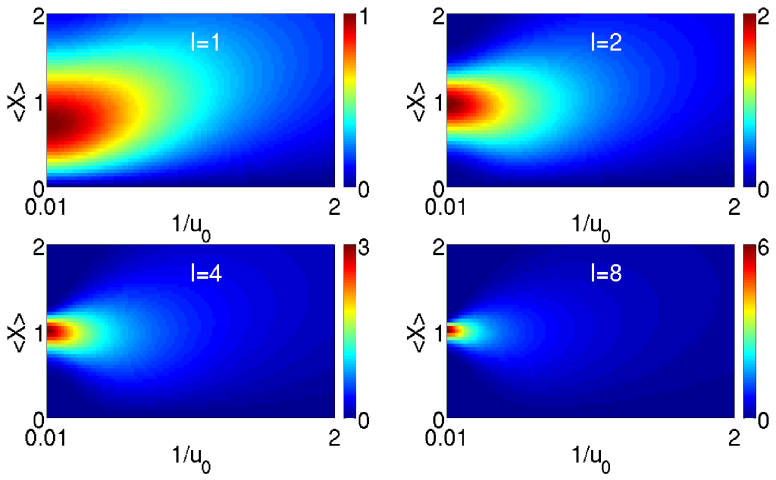

Fig. 2. Force experienced by the input beam for the case of a repulsive potential and various l values. The magnitude of the force increases with l. The maximum force becomes increasingly localized near $\langle X\rangle = 1$ due to the flattening of the index well with l.

Equation (4) is equivalent to the Newton equation, with the soliton as a pointlike particle located in $X = \langle X\rangle$, with an effective velocity $v = d\langle X\rangle/dZ$, the latter corresponding to the slope of the trajectory with respect to the axis Z. The effective velocity changes under the action of an effective force F given by the right hand side of Eq. (4), and is the average of the index gradient perceived by the soliton across its profile.
Expressing V_{eff} in a power series with respect to $X - \langle X\rangle$ we get

$$\frac{d^2\langle X\rangle}{dZ^2} = -p\int \psi\Big(\frac{\partial V_{\text{eff}}}{\partial X} + \frac{\partial^2 V_{\text{eff}}}{\partial X^2}(X-\langle X\rangle) + \frac{1}{2}\frac{\partial^3 V_{\text{eff}}}{\partial X^3}(X-\langle X\rangle)^2 + \dots\Big)\Big|_{X=\langle X\rangle} dX, \tag{5}$$

which can be cast in a more compact form as

$$\frac{d^2\langle X\rangle}{dZ^2} = p\sum_{m=0}^{\infty} W_m(\langle X\rangle)\langle \xi^m\rangle_\psi \tag{6}$$

by setting $W_m(\langle X\rangle) = -\frac{1}{m!}\frac{\partial^{m+1}V_{\text{eff}}}{\partial X^{m+1}}\Big|_{X=\langle X\rangle}$, with $\xi = X - \langle X\rangle$ and $\langle \xi^m\rangle_\psi = \int \psi\xi^m dX$.

Figure 2 displays the force F calculated at a given section $z = \text{const}$ and acting on a fundamental soliton ($N = 1$) as a function of its width (inversely proportional to the amplitude u_0) and for different defect profiles (i.e., varying l); the soliton is positioned at various transverse positions $\langle X\rangle$. Owing to the even symmetry of the photonic potential, we limit our consideration to the case $X > 0$, retaining such hypothesis hereafter in the article. Consistently with physical intuition, the force experienced by a narrow soliton is maximum when the latter is located on the largest gradient of the linear perturbation $n_L(X)$, its position being denoted as X_m; for a wide soliton the peak force reduces and shifts towards larger $\langle X\rangle$ due to the spreading of the wavefunction ψ. In addition, the largest absolute force increases and becomes localized in a narrower spatial region versus l.
We now consider narrow solitons in order to simplify Eq. (6): in this limit the force acting on the beam can be expressed as

#191688 - $15.00 USD Received 3 Jun 2013; revised 17 Jul 2013; accepted 20 Jul 2013; published 29 Jul 2013

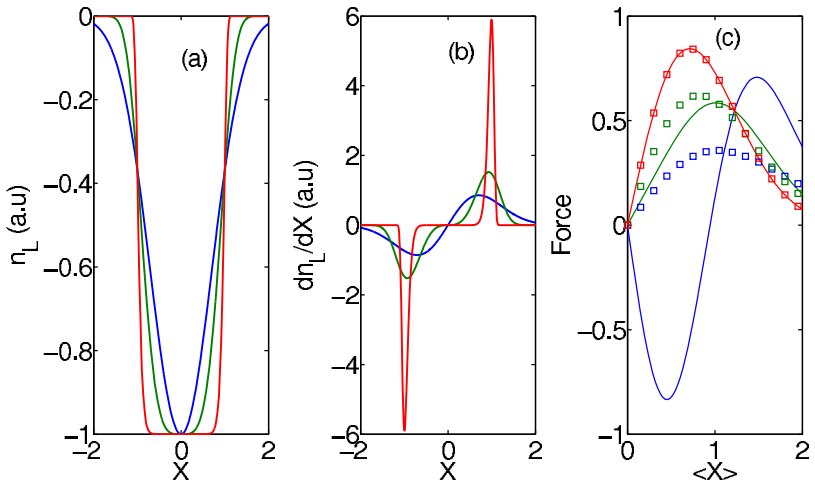

Fig. 3. (a) Refractive index well for $l = 1, 2, 8$. The index well flattens with l (top to bottom). (b) Corresponding refractive index gradient (top to bottom in the left half). (c) Comparison of force as given by Eq. (6) (symbols) and by Eq. (7) (solid lines) for $l = 2$, $u_0 = 1$, 2 and 10 (bottom to top).

$$\frac{d^2\langle X\rangle}{dZ^2} = p\left(W_0 + W_2\left\langle \xi^2\right\rangle\right). \tag{7}$$

Equation (7) states that, if the soliton is narrow with respect to the potential V_{eff}, its trajectory $\langle X\rangle(Z)$ depends on the beam position $\langle X\rangle$ and on its width w, the latter proportional to $\sqrt{\langle \xi^2\rangle}$ through a constant. In particular, Eq. (7) predicts the saturation of the change in soliton trajectory at high powers: in this regime the soliton motion is solely determined by the linear distribution n_L, quite a counterintuitive result. Hereafter, in the computations, we assume that the soliton waist (or equivalently its amplitude) does not change in propagation. Even though the Ehrenfest theorem can be generalized to a set of dynamical equations for all the moments, their form is quite cumbersome and hampers a simple physical interpretation. While reasonably simple equations can be derived for $\left\langle \xi^2\right\rangle$, their solutions strongly depend on the specific nonlinearity and will be investigated in future work.

Figures 3(a)-(b) shows the refractive index distribution and its gradient dn_L/dX for various l, with the gradient proportional to $W_0(\langle X\rangle)$. The comparison between complete and simplified formulae is plotted in Fig. 3(c): it is apparent that for broad solitons ($u_0 = 1$ and 2) the two approaches do not match, whereas for narrow solitons ($u_0 = 10$) they yield an equal force. In other words, the force from Eq. (6) is well approximated by just the W_0 term for a narrow soliton, whereas the terms depending on W_2 and W_m with $m > 2$ become non-negligible for a wider soliton.

In essence, the soliton dynamics depends markedly on the distribution of the photonic potential; for $\Delta > 0$ the light beam is attracted by the defect core, eventually leading to soliton trapping, whereas for $\Delta < 0$ the beam is repelled. In the next section we examine two kinds of defects and present their salient features on soliton propagation.

3. Fundamental soliton dynamics

Hereby we address the interactions of fundamental solitons (i.e., $N = 1$) with the linear inhomogeneity n_L by means of standard FD-BPM (Finite Difference Beam Propagation Method)

#191688 - $15.00 USD Received 3 Jun 2013; revised 17 Jul 2013; accepted 20 Jul 2013; published 29 Jul 2013

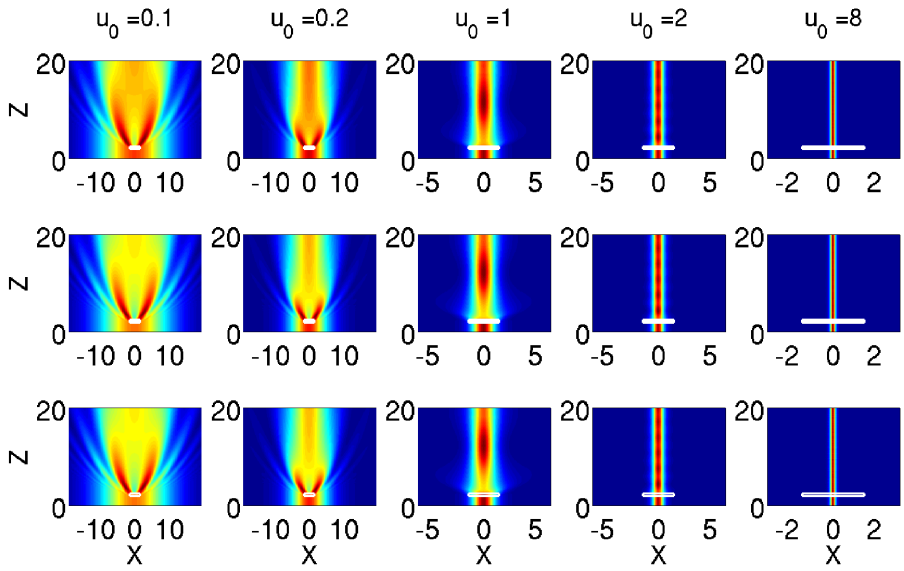

Fig. 4. Beam intensity evolution for $l = 1$ (top), $l = 4$ (middle) and $l = 8$ (bottom) for various u_0. Here $d = 0.5$, $Z_0 = 2.25$, $\Delta = -1$ and the beam is launched at $\langle X \rangle_0 = 0$.

simulations. We note that for $N = 1$ the soliton normalized power P, defined as $P = \int |u|^2 dX$, scales linearly with u_0 due to the dependence of the soliton width on its own amplitude. Photonic potentials of various transverse profiles, from Gaussian to flat-top, can be simulated by varying the super-Gaussianity parameter l. The boundaries of the refractive distribution n_L become increasingly abrupt as l gets larger, with the core region getting flatter and flatter. Various refractive wells for different l are graphed in Fig. 3(a) for a repulsive defect, together with the corresponding index gradients in Fig. 3(b), the latter becoming increasingly localized around $X = |1|$ for large l.

3.1. *Repelling potential*

In this section we take $\Delta < 0$, i.e., the potential "repels" light. Figure 4 shows the calculated soliton propagation for various amplitudes u_0 and three l, with a fixed d much shorter than the Rayleigh length of the beam; the soliton is launched in $\langle X \rangle_0 = 0$, i.e., on the symmetry axis of the defect. In agreement with Fig. 2, when the beam is injected at the center of the photonic potential the force acting on it is zero regardless of l, the latter feature holding valid even for attracting defects (i.e., independent on the sign of Δ). A more complicated beam dynamics takes place after the interaction with the defect. For narrow solitons (e.g. $u_0 > 1$ in Fig. 4) the phase modulation impressed on the beam across X is nearly uniform and the soliton profile remains substantially unaffected by the potential. For wide solitons (e.g. $u_0 \leq 1$ in Fig. 4), conversely, the defect induces an appreciable transverse phase modulation and power coupling with diffractive modes, in agreement with inverse scattering theory [37]. Photonic potentials of small extent along Z permit the soliton to survive but with a lower peak (otherwise stated, the soliton becomes wider). Since higher l correspond to larger index gradients (see Fig. 3(b)), the net result is a dissimilar beam breakup immediately outside the defect (e.g. $u_0 \leq 1$ in Fig. 4).

When the input beam is not collinear with the symmetry axis of the potential, the force does not vanish. Figure 5 shows the calculated beam evolution when $\langle X \rangle_0 = 1$ for $l = 1, 4, 8$ and various input powers. Analogously to the case $\langle X \rangle_0 = 0$, narrow solitons almost retain their

#191688 - $15.00 USD Received 3 Jun 2013; revised 17 Jul 2013; accepted 20 Jul 2013; published 29 Jul 2013

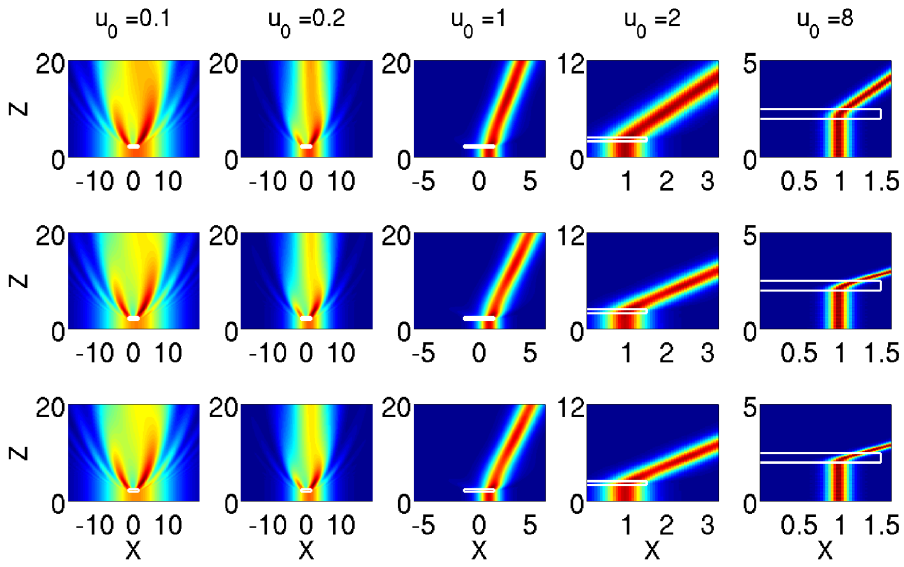

Fig. 5. Beam intensity evolution for $l = 1$ (top), $l = 4$ (middle) and $l = 8$ (bottom) for various u_0. Here $d = 0.5$, $Z_0 = 2.25$, $\Delta = -1$ and the beam is launched at $\langle X \rangle_0 = 1$.

profile after the interaction even if propagating in a different direction, whereas wide solitons lose power due to coupling to radiation. Furthermore, consistently with Fig. 2, wide solitons are nearly undeflected as positive and negative phase gradients cancels each other out when integrated across their profile.

Figure 5 clearly shows that soliton deflection depends on l, as expected. To better quantify soliton deflection and its dependence on power and l we introduce the output velocity $v_{\text{out}} = \left[\langle X \rangle (Z_f) - \langle X \rangle (Z_i)\right] / \left(Z_f - Z_i\right)$, where $Z_f, Z_i \gg Z_0 + d$ in order to ensure soliton stabilization after the interaction with the inhomogeneity. In physical coordinates, v_{out} is related to the exit angle θ of the soliton via $\theta = \arctan\left[v_{\text{out}}/(k_0 n_0 w_p)\right]$. Figure 6 displays both analytical (via Eq. (7), solid lines) and numerically calculated (symbols) v_{out} versus u_0 for various l and $\langle X \rangle_0$. Whatever the photonic potential, the soliton trajectories exhibit an asymptotic trend at high powers, in agreement with Eq. (7) as we are in the particle-like regime [17]. For large solitons (low u_0) Eq. (7) fails to model the output angle as we are in the wave-like regime: the exact Eq. (6) has to be employed for a correct prediction of the trajectory. The overall behavior of v_{out} versus u_0 strongly depends on the input position. The deflection v_{out} is monotonic and saturates for $\langle X \rangle_0$ in the neighbouring of X_m, i.e., in the proximity of the peak index gradient $(dn_L/dX)_{\max}$; conversely, for solitons launched far away from X_m, v_{out} first increases and then decreases versus power, with a local maximum. This is qualitatively maintained for various l, as well, and can be readily interpreted by looking at the right hand side of Eq. (4), i.e. the global force F: when the soliton is launched at the maximum index gradient, the overlap with the region of highest $|dn_L/dX|$ gets larger as the soliton shrinks; conversely, when the input soliton is slightly displaced from X_m, narrower solitons imply a lower overlap with the peak of the gradient; eventually, for input solitons far away from X_m, v_{out} tends to flatten versus u_0 owing to the negligible beam overlap with the core of the photonic potential.

Figure 6 also shows that, for a fixed l, v_{out} is largest for $\langle X \rangle_0 \approx 1$, whereas it reduces when moving away from this position. In fact, from Fig. 3(b) it can be appreciated that the largest index gradient $|dn_L/dX|$ gets increasingly closer to $X = 1$ as l gets larger (in other words $X_m \to 1$), its location given by $d^2 n_L/dX^2 = 2n_L(X)\Delta[(2l-1)X^{2(l-1)} - 2lX^{4l-2}] = 0$. Since the maximum

#191688 - $15.00 USD Received 3 Jun 2013; revised 17 Jul 2013; accepted 20 Jul 2013; published 29 Jul 2013

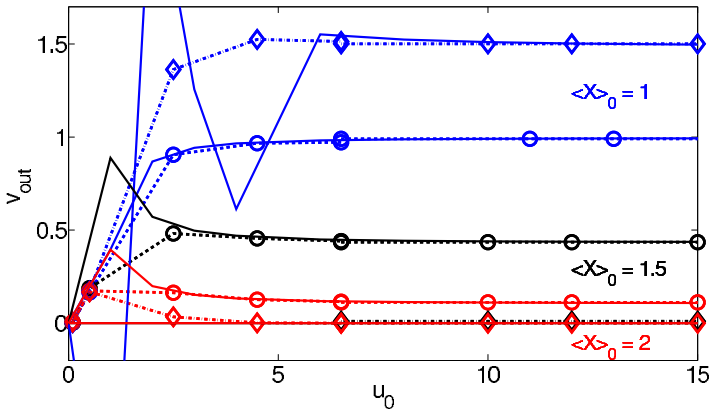

Fig. 6. Soliton deflection versus soliton amplitude u_0 for $\langle X\rangle_0 = 1$ (blue), 1.5 (black) and 2 (red) for $l = 1$ (dashed line (○)) and 4 (dashed-dotted line (◇)). Here $\Delta = -3$ and $d = 0.5$. Symbols correspond to numerical result and solid line corresponds to analytical which overlaps for large u_0.

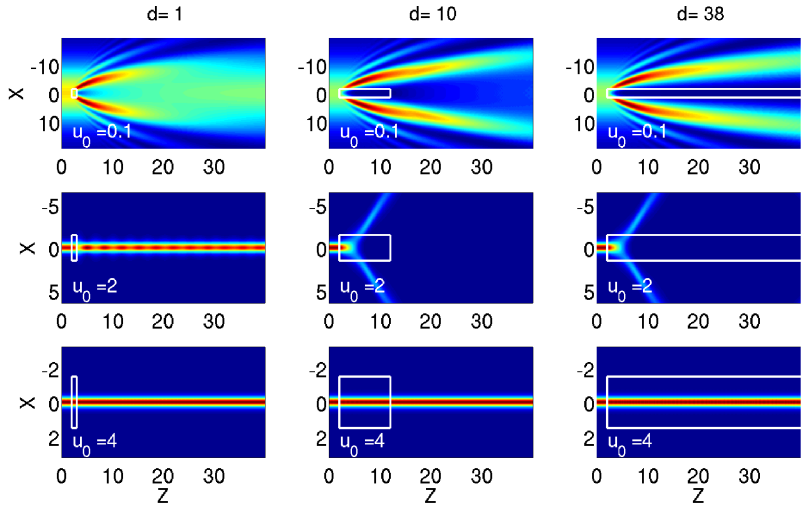

Fig. 7. Intensity evolution for various u_0, d and $\Delta = -1$. The white rectangles represent the potential.

#191688 - $15.00 USD Received 3 Jun 2013; revised 17 Jul 2013; accepted 20 Jul 2013; published 29 Jul 2013

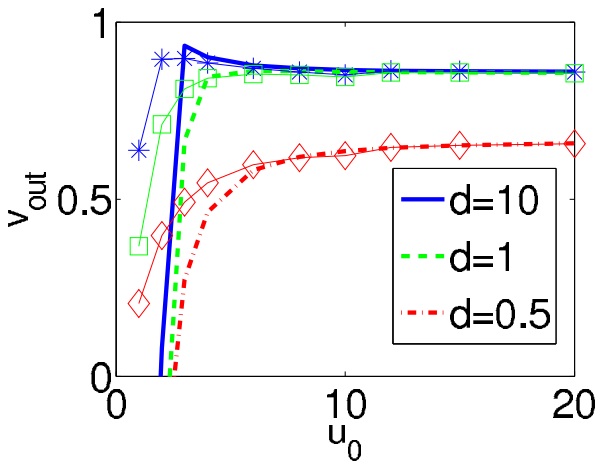

Fig. 8. Soliton deflection versus power for $l = 2$, $\langle X \rangle_0 = 1$, $\Delta = -1$ and $d = 0.5$ ($\Diamond$), 1 ($\Box$) and 10 ($*$) computed via Eq. (7). Symbols are numerical results and the lines corresponds to analytical predictions.

$|dn_L/dX|$ increases with l, the maximum v_{out} over all possible input positions grows with l; this implies that an index defect with sharp boundaries (e.g. $l = 8$) can steer the soliton more than a defect with a smooth variation (e.g. $l = 1$) for a given Δ. As discussed earlier, the index well increasingly flattens versus l, resulting in a negligible force for $|\langle X \rangle_0| \neq 1$ and negligible steering for beams much narrower than the defect.

In summary, the transverse profile of a defect short along Z does not affect the soliton trajectory as long as the potential is symmetric with respect to the soliton axis. The profile becomes relevant on soliton steering when the beam input is away from the core of the defect, producing beam breakup for wide solitons. Moreover, for a given photonic potential, soliton deflection depends on the launch position: input solitons centered by the maximum refractive index gradient will always experience the maximum force and be steered away for increasing input powers; for solitons on either side, conversely, the deflection angle can increase, reach a maximum and eventually decrease with power. The defect profile shifts the peak of the refractive index gradient and affects the steering angle.

Finally, to completely characterize the system, we consider the role of longitudinally extended defects on soliton dynamics. We take potentials of length ranging from $d = 0.5$ to 38 and study the soliton evolution along Z. We fix $l = 2$ and $\langle X \rangle_0 = 0$. Figure 7 displays the soliton propagation for various lengths d and three input powers, $u_0 = 0.1, 2$, and 4, respectively, such as to capture the essential physics. For short defects the beam dynamics goes from multiple fringes to a soliton versus power; for increasing d the beam splits into equal halves, each carrying equal amounts of power at opposite angles: at small powers the linear potential dominates over the nonlinear well due to self-focusing and the soliton is destroyed; in the opposite limit, self-focusing overruns the defocusing due to n_L and the soliton propagates nearly unperturbed [38]. Clearly, the longer the defect the stronger is the defocusing action.

The extension d also affects soliton deflection v_{out}: Fig. 8 plots v_{out} when $\langle X \rangle_0 = 1$, i.e., when the force F is maximum. The deflection v_{out} tends to saturate at high powers for all d, similar to Fig. 6. Moreover, beyond a certain d the asymptotic v_{out} clamps to the same value as the soliton gets "pushed out" of the potential after some propagation (as in Fig. 5, rightmost panels), this upper d being smaller for narrower solitons. The numerical results (symbols) agree quite well with the analytical predictions from Eq. (7) in the particle-like regime (lines), in full analogy

#191688 - $15.00 USD Received 3 Jun 2013; revised 17 Jul 2013; accepted 20 Jul 2013; published 29 Jul 2013

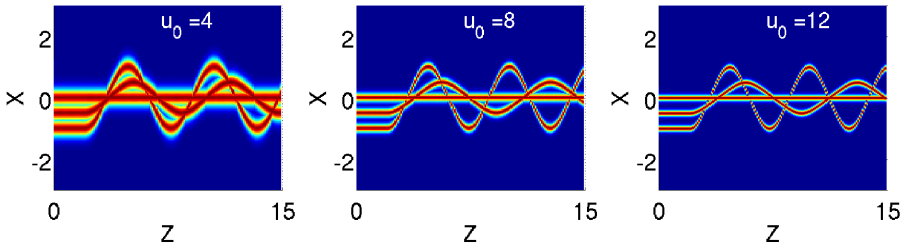

Fig. 9. Beam intensity evolution for a defect with $d = 15$, $l = 2$, $\Delta = 1$ when the beam is launched at $\langle X \rangle_0 = 0, 0.5, 1$ for u_0 varying from 4 to 12, as marked.

with Fig. 6 as expected.

3.2. Attracting potential

An attracting inhomogeneity $\Delta > 0$ gives rise to a richer dynamics in soliton propagation as compared to a repelling defect. In Fig. 9 the input power is chosen such that the soliton behaves as a particle. The beam can be trapped inside the potential and undergo transverse oscillations (for a long enough well along Z), also depending on the input position.

The oscillation period varies with both input position and power. Figure 9 illustrates the beam evolution for solitons of various powers launched in different transverse locations of a defect with $d = 15$. In all simulations $l = 2$. As power increases the period decreases for beams injected by the maximum refractive index gradient; on either side of this maximum the period increases. Noteworthy, the oscillation period becomes constant for very narrow solitons in the particle-like limit (see Eq. (7)); hence, it is possible to steer solitons at desired angles by controlling the power and the defect length. For short potentials the deflection angle resembles that due to a repelling potential except for the sign, unless the period gets small enough to yield soliton trapping within a longitudinally extended defect (see, e.g. experimental and numerical results on trapping of nonlocal solitons in liquid crystals [15, 39]).

Figures 10(a)-(b) shows the soliton trajectory and the corresponding radius versus Z for beams of various input powers launched in $\langle X \rangle_0 = 1$, with $d = 0.5$. Analogously to the previous cases, the soliton trajectories for large amplitudes u_0 are well modeled by Eq. (7). Noteworthy, the soliton width is not appreciably affected by the linear potential. In this case solitons undergo half oscillation: for larger d the deflection v_{out} can span from positive to negative values as power varies, since the oscillation period depends on soliton power/radius (see Fig. 9). As the solitary beam can emerge on either side of the defect, this can be effectively used to achieve wide angle steering (see, e.g., [30]). Another approach to change the sign of v_{out} consists in changing the peak Δ of n_L, varying in turn the oscillator strength responsible for soliton trapping. Results for v_{out} in the case $d = 10$ are plotted in Fig. 10(c): the overall deflection can be either positive or negative; Figs. 10(d)-(f) displays the corresponding soliton trajectories. Thus, for a given input, an attracting photonic potential allows to approximately double the overall steering angle versus power with respect to a repelling defect.

4. Breathers

In this section we extend the former results to a breather soliton with $N = 2$. We concentrate on the case $\Delta > 0$, i.e., a trapping defect. First, we investigate breathing oscillations inside the potential, trying to determine whether and when Eq. (7) is valid for breather solitons: in fact, the radius (width) of these nonlinear waves changes in propagation, so the force acting on them is not constant along Z, even if the linear potential n_L does not appreciably affect the beam

#191688 - $15.00 USD Received 3 Jun 2013; revised 17 Jul 2013; accepted 20 Jul 2013; published 29 Jul 2013

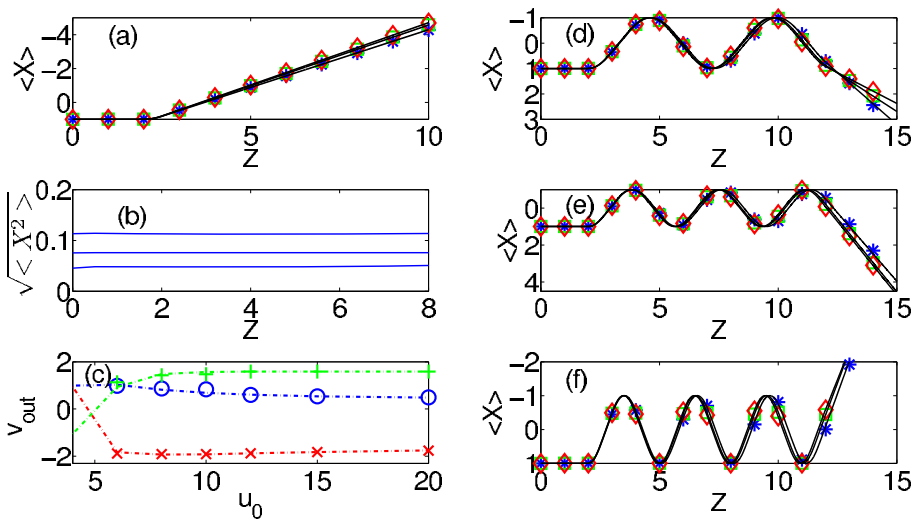

Fig. 10. (a) Soliton trajectory and (b) corresponding beam radius for $d = 0.5$ and $\Delta = 1$. (c) Variation in output angle with u_0 for $d = 10$ and $\Delta = 1$ ($\circ$), 2 ($+$) and 3 (X) with the corresponding trajectories plotted in (d-f). In panels (a,d,e,f) solitons are launched in $\langle X\rangle_0 = 1$ with $l = 2$ and $u_0 = 8$ ($*$),12 ($\square$) and 20 ($\diamond$). Symbols correspond to numerical and lines correspond to theoretical predictions.

width. To this extent we need to find breathing solitary oscillations in unperturbed Kerr media; breather evolution along Z for $N = 2$ is given by [35]

$$u(X,Z) = 4u_0 e^{\frac{iu_0^2 Z}{2}} \frac{\cosh(3u_0X) + 3\cosh(u_0X)e^{4iu_0^2Z}}{\cosh(4u_0X) + 4\cosh(2u_0X) + 3\cos(4u_0^2Z)}. \tag{8}$$

From Eq. (8) we can compute both the oscillation amplitude and period versus u_0, as shown in Fig. 11(a). u_0 identifies each member of the soliton family, as in the case $N = 1$; however, for a given u_0, the power of the breather (Eq. (8)) is four times larger than the power of the fundamental soliton because of the factor N in the amplitude. We also simulated numerically the breather evolution in a trapping defect with $\Delta = 1$ and $d \to \infty$, i.e., infinitely extended. Using Eq. (7) with the breather width computed from Eq. (8), we can find the trajectory in the limit of narrow solitons, assuming that n_L does not affect substantially their transverse size. We then compare the theoretically calculated trajectories of breathers launched for various u_0 in various locations $\langle X\rangle_0$ with the corresponding numerical results, see Figs. 11(b)-(c): these approaches are in good agreement for widths $1/u_0$ up to 0.1: beyond such value the beam deviates from particle-like due to energy emission from the breather; depending on the amount of shed energy this energy interacting with the defect boundary, can either propagate in a bound form with the main soliton (Fig. 11(d)) or can evolve as an independent wavepacket.

We then demonstrate the steering of a breather soliton in a finite defect of length d. In full analogy with the fundamental soliton, the oscillation period inside the linear trap depends on the amplitude as well as on the input position: controlling the longitudinal extension d, the output angle of the emerging breather soliton can be varied. We numerically studied the propagation of breathers much narrower than the photonic potential (i.e., in the particle-like limit) launched in $\langle X\rangle_0 = 0.5$. Figure 12 shows power controlled steering of breathers. The output angle (related to the equivalent velocity v_{out} via an arctan function) can be further controlled by varying the defect length. For $d = 10$, four breather solitons of amplitudes $u_0 = 20$, 14.29, 12.5 and 10.00,

#191688 - $15.00 USD Received 3 Jun 2013; revised 17 Jul 2013; accepted 20 Jul 2013; published 29 Jul 2013

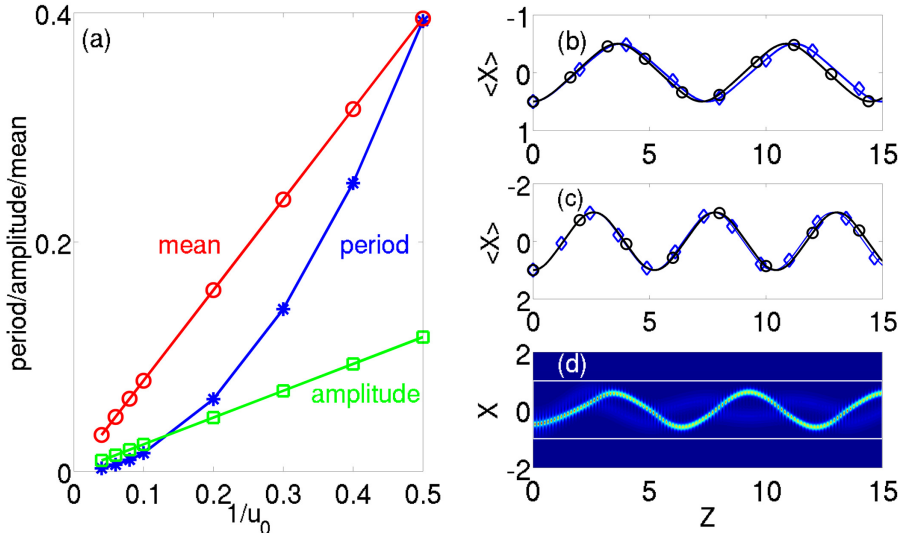

Fig. 11. (a) Breather soliton properties: oscillation period (∗), amplitude (□) and mean radius (○) versus inverse amplitude $1/u_0$. (b-c) Theoretical (solid line) and numerical (symbols) trajectories for breather solitons of widths 0.05 (blue diamond) and 0.1 (black circles) launched in (b) $\langle X\rangle_0 = 0.5$ and (c) $\langle X\rangle_0 = 1.0$. (d) Evolution profile of breather soliton in propagation for $\langle X\rangle_0 = 0.5$ for initial radius 0.3 showing energy escape. The theoretical results here are derived by solving jointly Eq. (7) and Eq. (8). Here $\Delta = 1$.

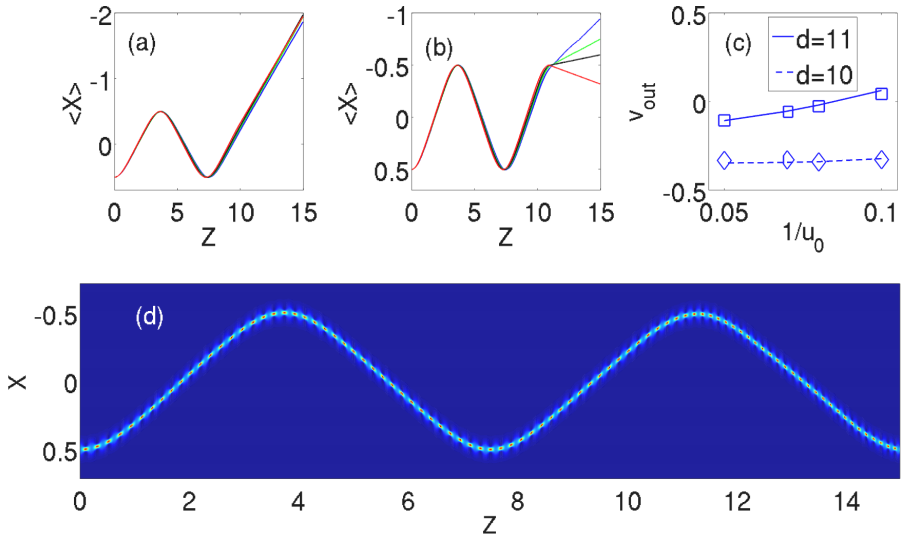

Fig. 12. Trajectories of breathers with power $u_0 = 20$ (blue), 14.29 (green), 12.5 (black) and 10.0 (red) launched in $\langle X\rangle_0 = 0.5$ for defects of length (a) $d = 10$ and (b) $d = 11$. (c) Corresponding velocities (symbols) and comparison with theoretical results (lines). (d) Propagation of a breather of width 0.05 in an infinitely long potential.

#191688 - $15.00 USD Received 3 Jun 2013; revised 17 Jul 2013; accepted 20 Jul 2013; published 29 Jul 2013

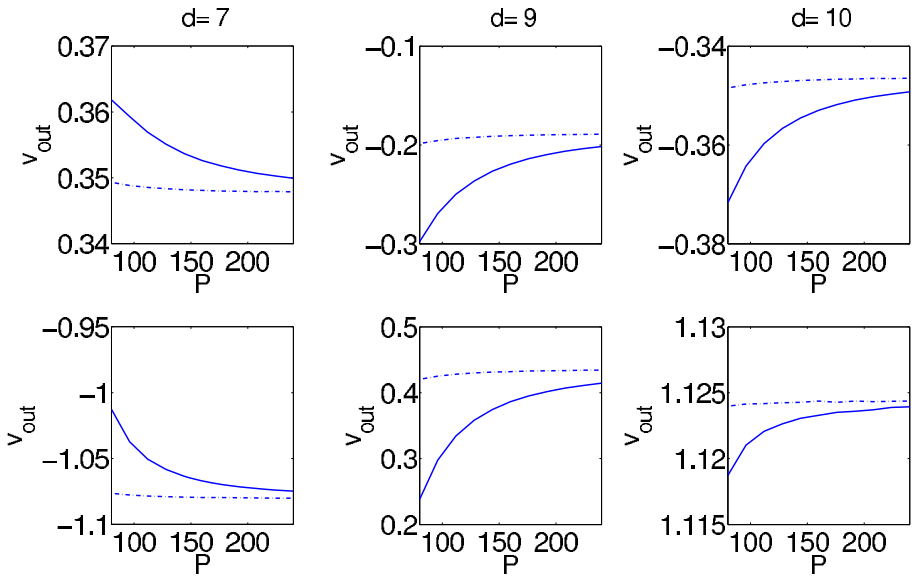

Fig. 13. Comparison of velocity variation of fundamental (dashed lines) and breather (solid lines) solitons versus amplitude for various defect lengths (along columns) when launched in $\langle X\rangle_0 = 0.5$ (top) and $\langle X\rangle_0 = 1$ (bottom).

respectively, propagate almost collinearly with very small difference in exit trajectory (angle), see Fig. 12(a). For the length $d = 11$ the output angles drastically change with excitation, as visible in Fig. 12(b). The corresponding soliton velocities v_{out} following the defect are plotted in Fig. 12(c) and compared with the analytical results, with excellent agreement.

Finally, in Fig. 13 we compare the steering of fundamental and breather solitons. For a meaningful comparison we consider the same power P for both solitons, i.e. with N=1 and N=2, respectively. In terms of u_0, the two beams have the same power when the amplitude of the fundamental soliton is 4 times larger than the amplitude of the breather; this implies that, at the input, the fundamental soliton is 4 times narrower than the breather soliton. We stress that, even if the breather size changes along Z, its mean width is close to the value $1/u_0$ (i.e., the soliton width in $Z = 0$, point where the radius is maximum), as shown by the behavior of mean width versus u_0 plotted in Fig. 11. From these considerations we can expect that, for a given power, due to its smaller radius a fundamental soliton is much closer to saturation than a breather soliton: Fig. 13 confirms such prediction, showing how a breather soliton undergoes a much larger deflection than a fundamental soliton.

5. Conclusions

We have studied the interaction of (one dimensional) spatial optical solitons with a linear photonic potential embedded in a nonlinearly-homogeneous Kerr medium, i.e. a finite perturbation of the linear refractive index. Depending upon the ratio between the width of the input soliton and the width of the defect, different propagation regimes were observed. When the ratio is large, i.e. when a wide soliton is launched at the input, the defect induces strongly inhomogeneous phase modulations across the transverse profile of the soliton, eventually producing its breakup into multiple fringes. When the input soliton is substantially narrower than the defect, it survives the perturbation and undergoes deflection. In intermediate cases, a deflected soliton emerges the interaction but with a lower amplitude due to power transfer to radiation.

#191688 - $15.00 USD Received 3 Jun 2013; revised 17 Jul 2013; accepted 20 Jul 2013; published 29 Jul 2013

This phenomenology, jointly with the well known dependence of the soliton width with power, entails power-tunable steering of self-confined light beams and the corresponding waveguides. For a repelling potential the steering occurs in one half of the defect plane, whereas for an attracting potential solitons can be steered in either halves. Using the Ehrenfest theorem we can predict the evolution of width and position of narrow solitons, in good agreement with numerics. We have characterized the role of transverse profile and longitudinal extension of both repelling and attracting index wells on the soliton dynamics, depending on initial launch position and excitation levels. These results illustrate novel avenues for soliton steering and deflection using linear perturbations of refractive index, paving the way to the use of electro-optic or thermo-optic effect for complete control on soliton trajectories and routing of the associated waveguides. Finally, our results are not limited to Kerr media, but can be easily extended to other nonlinearities, accounting e.g. for saturating as well as nonlocal responses. The use of optical nonlinearities in soft matter (e. g. nonlocal reorientation in molecular media) could readily permit the actual demonstration of various steering regimes employing stable sub-mW two-dimensional self-confined beams (see, e.g. [40]), extending soliton (and soliton waveguide) deflection to the full three-dimensional space.

Acknowledgments

JCP and AA gratefully acknowledge support from grant FCT SFRH/BPD/77524/2011 and from Regione Lazio, respectively.

#191688 - $15.00 USD Received 3 Jun 2013; revised 17 Jul 2013; accepted 20 Jul 2013; published 29 Jul 2013